

# Parity and time-reversal invariant Ising spin ordering

Yue Yu,<sup>1,2</sup> Jin Matsuda,<sup>3</sup> Hikaru Watanabe,<sup>4</sup> Ryotaro Arita,<sup>5,6</sup> and Daniel F. Agterberg<sup>1</sup>

<sup>1</sup>*Department of Physics, University of Wisconsin–Milwaukee, Milwaukee, Wisconsin 53201, USA*

<sup>2</sup>*School of Physics and Astronomy, University of Minnesota, Minneapolis, Minnesota 55455, USA*

<sup>3</sup>*Department of Applied Physics, The University of Tokyo, Hongo, Bunkyo-ku, Tokyo 113-8656, Japan*

<sup>4</sup>*Department of Applied Physics, Hokkaido University, Sapporo, Hokkaido 060-8628, Japan*

<sup>5</sup>*Department of Physics, The University of Tokyo, Hongo, Bunkyo-ku, Tokyo 113-0033, Japan*

<sup>6</sup>*RIKEN Center for Emergent Matter Science, 2-1 Hirosawa, Wako, Saitama 351-0198, Japan*

The interplay of antiferromagnetic order, momentum-dependent Bloch spin-splitting, time-reversal (T), and parity (P) symmetries in non-relativistic systems has emerged as a central theme for spintronics. Two well-known examples are P-preserving and T-violating altermagnets and P-violating and T-preserving odd-parity magnets. These both exhibit an Ising, or uniaxial, Bloch spin-splitting. Here we introduce a new class of coplanar AFMs that generate a P and T symmetric, translation-invariant Ising spin order in real space. Naively, such AFMs are not expected to exhibit unusual phenomena. Here we show that the spin-rotational symmetry breaking generated by these AFMs allows: pure non-relativistic longitudinal (or transverse) spin-conductivities, the generation of non-relativistic altermagnetic spin-splittings through circularly polarized light, and the generation of non-relativistic odd-parity spin-splittings through parity symmetry breaking, by, for example, applied electric fields. We identify 16 candidate materials in the Magndata database for which our theory applies and provide effective microscopic models and DFT-based results that highlight the large emergent responses.

*Introduction:* Altermagnetism has recently emerged as a central topic in quantum magnetism[1–5]. Like ferromagnetism, it exhibits collinear spin ordering, preserves lattice translation, breaks time-reversal  $T$  symmetry, and preserves inversion  $P$  symmetry. The  $(P, T) = (+, -)$  property leads to nonrelativistic even-parity Ising spin splittings in momentum space[6], that enables spin-transport[7, 8] and spin caloritronics[9]. When spin-orbit coupling (SOC) is present, altermagnets can also generate anomalous Hall transport[10, 11].

Driven by altermagnetism, interest in other unconventional magnets has also grown[12–15], notably odd-parity (or  $p$ -wave) magnets[16–20]. These antiferromagnets (AFMs) break lattice translational symmetry with non-collinear spin orderings. These AFMs induce a translational invariant spin order that is  $(P, T) = (-, +)$ , allowing odd-parity Bloch spin splittings. Depending on whether the AFM is coplanar or non-coplanar, the induced spin splittings can be Ising-like [16–19] or non-Ising-like[20]. As nonrelativistic analogues of Ising and Rashba SOC, they can play a significant role in spintronics[21–24].

PT-symmetric magnets, with  $(P, T) = (-, -)$ , have also received renewed scrutiny [25–27]. The  $PT$  symmetry guarantees doubly-degenerate bands, hiding the spin-charge locking[28]. Bloch spin splittings can be unlocked by spin-independent perturbations that break  $P$  or  $T$  (Top-right of Fig.1). Ferroelectricity, electric fields, or surface  $P$ -breaking can generate even-parity ferromagnetic[29] or altermagnetic[29–35] spin splittings. Circularly polarized light can generate odd-parity Ising spin splittings[36–39].

In this work, we reveal the final class of Ising spin orders defined under  $(P, T)$  symmetry. They are even under

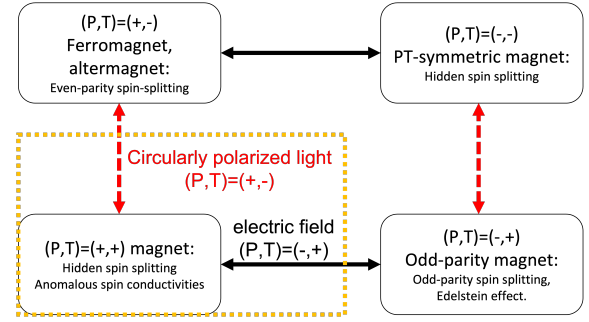


FIG. 1. The four classes of translationally-invariant spin orders under  $(P, T)$  symmetries. This paper covers the yellow dotted region.

both inversion and time-reversal symmetries:  $(P, T) = (+, +)$ , yet they break spin-rotational symmetry. Generally,  $(P, T) = (+, +)$  symmetric order, like  $(P, T) = (-, -)$  order, forbids spin-splittings in momentum space. This suggests that such ordering will be uninteresting from the spintronics perspective. Here we argue that this is not the case. In particular, coplanar AFMs can induce an even parity vector spin chirality (VSC) that can be interpreted as a variant of a more usual even parity  $\mathbf{L} \cdot \mathbf{S}$ -like SOC. Since usual SOC is known to underlie spin-conductivities [40–42], this even-parity VSC will also generate non-zero spin-conductivities. Importantly, as non-relativistic variants of the more usual  $\mathbf{L} \cdot \mathbf{S}$ -like SOC, the resultant spin-conductivities can be parametrically larger and can hence play a key role in spintronics.

In addition, since the even-parity VSC originates from symmetry breaking, the resultant spin-conductivities need not be transverse as is typical for  $\mathbf{L} \cdot \mathbf{S}$  SOC [40–43].

Here we find AFMs with large transverse non-relativistic spin conductivities. We also find ferroaxial VSCs, in which there is only non-relativistic longitudinal spin conductivities. In contrast to other emergent spin current responses, such as in  $\text{Mn}_3\text{Sn}$  [44, 45] and altermagnetic materials [46–49], in which time-reversal symmetry is broken, here only time-reversal even spin responses appear, which are impurity scattering independent [50, 51]. In addition, while  $(P, T) = (+, +)$  magnets exhibit no spin-splitting, we show circular polarized light generates an even parity spin splitting, and electric fields generate an odd-parity spin splitting, allowing control for spintronics applications. The relationships among the four classes of  $(P, T)$  materials are summarized in Fig. 1.

AFM order can generate  $(P, T) = (+, +)$  order in two ways [52]. In the first, which applies to collinear AFMs, the  $(P, T) = (+, +)$  order is spin-scalar, and is hence orbital-active. The case when collinear AFM order breaks mirror symmetries, giving orbital-active ferroaxial order, has been examined recently [52] and shown to give rise to a third-order non-linear Hall effect. Here we focus on the second possibility, in which coplanar AFM order gives rise to spin-active  $(P, T) = (+, +)$  arising from an even-parity Ising VSC. This order is conceptually similar to the odd-parity magnetic Ising order found in coplanar AFM order [16–19]. The key difference is that the VSC for odd-parity magnetism is odd-parity, and here we consider even-parity VSC.

In this work, we present a group-theory-based microscopic template for  $(P, T) = (+, +)$  spin-active magnets induced by 166 period-doubling AFMs and provide explicit microscopic models for these. We apply both phenomenological and microscopic analysis to demonstrate the non-zero transverse and longitudinal non-relativistic spin conductivities from the  $(P, T) = (+, +)$  spin-active magnets. Using first-principles calculations, we show that the non-relativistic spin Hall conductivity in  $\text{U}_2\text{Ni}_2\text{In}$  is comparable to that of Pt, providing a realistic demonstration of the utility of spin-active magnets. We further show that  $(P, T) = (+, +)$  spin-active magnets give rise to controllable spin-splittings through the application of electric fields or circularly polarized light.

*Symmetry Arguments:* Prior to presenting general symmetry-based arguments underlying the spin-active  $(P, T) = (+, +)$  order, we give a simplified example that highlights the essential elements. Figure 2 illustrates the simplest example of a  $(P, T) = (+, +)$  spin-active magnet, induced by a coplanar period-doubling AFM. The nonmagnetic unit cell contains two atoms with magnetic moments  $\mathbf{S}_{1,2}$ . The  $(P, T) = (+, +)$  magnet is characterized by the VSC order parameter  $\mathbf{S}_1 \times \mathbf{S}_2$ . This translationally invariant macroscopic parameter in spin space is relevant for spintronics applications. This spin-vector is time-reversal invariant, as time-reversal symmetry flips both spins. Consideration of inversion symmetry naturally leads to three cases in Fig.2. In the first case,

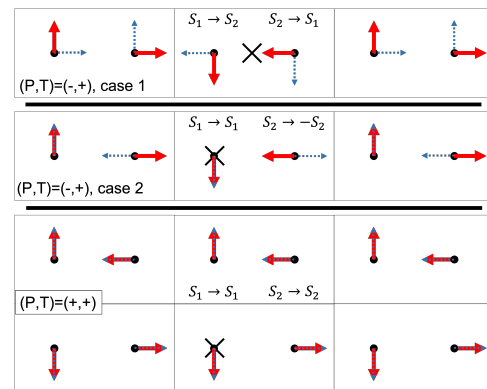


FIG. 2. Spin configuration of the coplanar AFM state, denoted by red solid arrows. Its inversion pair is illustrated by blue dashed arrows. The inversion center is at the X mark. Black solid lines denote the nonmagnetic unit cell. For  $(P, T) = (-, +)$  state, inversion symmetry acts non-trivially on the AFM[19], while for  $(P, T) = (+, +)$  state inversion is trivial.

inversion interchanges  $\mathbf{S}_1$  and  $\mathbf{S}_2$ . In the second case, inversion leaves  $\mathbf{S}_1$  unchanged but flips  $\mathbf{S}_2$ . Both results in an inversion-odd  $\mathbf{S}_1 \times \mathbf{S}_2$ , describing p-wave, or more generally, odd-parity magnets[19] with  $(P, T) = (-, +)$ . In contrast, for the third case, the inversion symmetry acts trivially on  $\mathbf{S}_{1,2}$ , and the resulting  $\mathbf{S}_1 \times \mathbf{S}_2$  is even under inversion, describing  $(P, T) = (+, +)$  spin-active magnets. While inversion symmetry is preserved, spin rotation symmetry is broken, and this leads to the non-vanishing spin conductivities and the field-controllable spin splittings discussed below.

Key to the above argument is the presence of two AFM orders  $\mathbf{S}_{1,2}$  that allow a non-vanishing VSC. From a symmetry perspective, this implies that the AFM order forms (at least) a two-dimensional (2D) representation (IR). For such a 2D IR, the coplanar AFM state can be stabilized through a single continuous phase transition [53]. It is possible to identify all space groups and AFM wavevectors that host the desired 2D IR. Specifically, period-doubling AFMs have wavevectors at time-reversal invariant momentum (TRIM). The trivial inversion operator needs to commute with all symmetries at these TRIM. We find that this happens in 166 2D IRs. We note that in general these 2D IRs are not restricted to cases with only two atoms per nonmagnetic unit cell (as was the case in Fig. 2). For systems with more atoms, the theory remains applicable with  $\mathbf{S}_1$  and  $\mathbf{S}_2$  now describing spin order across multiple atoms in the non-magnetic unit cell.

The AFM order parameter components  $\mathbf{S}_i \in \Gamma_{\mathbf{Q}} \otimes \Gamma_A^S$ , where  $\Gamma_{\mathbf{Q}}$  is a 2D IR under real-space symmetries at the TRIM  $\mathbf{Q}$ , and  $\Gamma_A^S$  is the vector IR under spin rotations (here we follow the notation of Ref.[54]). In the absence of SOC, symmetry arguments imply that the free energy for the order parameter  $(\mathbf{S}_1, \mathbf{S}_2)$  for all 166 theories can

be written

$$\begin{aligned}
f &= a(T) \sum_i \mathbf{S}_i \cdot \mathbf{S}_i + \beta_1 \left( \sum_i \mathbf{S}_i \cdot \mathbf{S}_i \right)^2 \\
&+ \beta_2 (2\mathbf{S}_1 \cdot \mathbf{S}_2)^2 + \beta_3 (\mathbf{S}_1 \cdot \mathbf{S}_1 - \mathbf{S}_2 \cdot \mathbf{S}_2)^2 \\
&+ \beta_4 (2\mathbf{S}_1 \cdot \mathbf{S}_2) (\mathbf{S}_1 \cdot \mathbf{S}_1 - \mathbf{S}_2 \cdot \mathbf{S}_2).
\end{aligned} \tag{1}$$

The quartic terms differ between the 166 theories. In particular,  $\beta_{1,2,3}$  always appear. The  $\beta_4$  term appears only if the two inner products  $\mathbf{S}_1 \cdot \mathbf{S}_2$  and  $\mathbf{S}_1 \cdot \mathbf{S}_1 - \mathbf{S}_2 \cdot \mathbf{S}_2$  carry the same symmetry, which happens when all the real-space symmetries take  $(\mathbf{S}_1, \mathbf{S}_2)$  to either  $\pm(\mathbf{S}_1, \mathbf{S}_2)$  or  $\pm(\mathbf{S}_2, -\mathbf{S}_1)$ .  $\beta_{1,2,3}$  are typically different; however, there exist examples when  $2\mathbf{S}_1 \cdot \mathbf{S}_2$  and  $\mathbf{S}_1 \cdot \mathbf{S}_1 - \mathbf{S}_2 \cdot \mathbf{S}_2$  belong to the same 2D IR. In these cases  $\beta_2 = \beta_3$ . The symmetry of  $\mathbf{S}_1 \cdot \mathbf{S}_2$  and  $\mathbf{S}_1 \cdot \mathbf{S}_1 - \mathbf{S}_2 \cdot \mathbf{S}_2$  for all 166 relevant 2D IRs is given in the SM (Table.I). The ground state solution depends upon the specific values of the  $\beta_i$  and is discussed in more detail in the End Matter. Generally, we find two possible collinear AFM states and a coplanar state for which the VSC order  $\mathbf{S}_1 \times \mathbf{S}_2$  is non-vanishing. Having established its existence, in the following, we turn our attention to the coplanar state with non-vanishing VSC order. In Ref.[52], we have discussed related collinear states that give rise to orbital active ferroaxial order.

*Spin Conductivities:* Since the  $(P, T) = (+, +)$  spin-active magnet breaks spin rotational symmetry, it can generate nonrelativistic spin conductivities given by  $J_i^l = \sigma_{ij}^l E_j$ . Here,  $J_i^l$  is a spin current along  $i$  with spin parallel to  $\hat{l}$ , and  $E_j$  is the electric field along  $j$ . Indices  $ijl$  can be determined by the symmetry of  $\mathbf{S}_1 \times \mathbf{S}_2$ .  $\mathbf{S}_1 \times \mathbf{S}_2$  transforms as  $(\Gamma_{\mathbf{Q}} \otimes_A \Gamma_{\mathbf{Q}}) \otimes \Gamma_A^S$ , where  $\otimes_A$  denotes an antisymmetric direct product. The appearance of the antisymmetric direct product  $\Gamma_{\mathbf{Q}} \otimes_A \Gamma_{\mathbf{Q}}$  follows from the antisymmetry of the cross product, and this governs the spatial symmetry of the VSC. Here, we have  $J_i^l \in \Gamma_V \otimes \Gamma_A^S$  and  $E_j \in \Gamma_V \otimes \Gamma_1^S$ , where  $\{x, y, z\} \in \Gamma_V$  is the polar vector representation under real-space operations. Spin conductivities thus transform as  $(\Gamma_V \otimes \Gamma_A^S) \otimes (\Gamma_V \otimes \Gamma_1^S) = (\Gamma_V \otimes \Gamma_V) \otimes \Gamma_A^S$ . Spin rotations require  $\hat{l} // \mathbf{S}_1 \times \mathbf{S}_2$ , real-space symmetries require  $\Gamma_{\mathbf{Q}} \otimes_A \Gamma_{\mathbf{Q}} \subset \Gamma_V \otimes \Gamma_V$ . Under time-reversal symmetry,  $J_i^l$ ,  $E_j$ , and  $\mathbf{S}_1 \times \mathbf{S}_2$  are all T-even, suggesting that the conductivity  $\sigma_{ij}^l$  is an even function of relaxation time [26, 50, 51, 55] and can be dissipationless.

Using the preceding symmetry analysis, we have determined nonrelativistic spin conductivities for all 166 2D IRs, as summarized in SI (Table.II). In addition, we further include 16 non-collinear AFM realizations from Magndata database[56]. We find that the most common spatial symmetries for  $\mathbf{S}_1 \times \mathbf{S}_2$  (that is  $\Gamma_{\mathbf{Q}} \otimes_A \Gamma_{\mathbf{Q}}$ ) are either  $A_{2g}$  or  $A_{1g}$  (in tetragonal and hexagonal point groups). As explained in the examples below, for  $A_{2g}$  symmetry, we find pure spin Hall conductivities ( $\sigma_{ij}^l = -\sigma_{ji}^l$ ), and for  $A_{1g}$ , we find pure longitudinal spin con-

ductivities ( $\sigma_{ii}^l$ ).

As a first example, consider space group 127 and with wavevector  $\mathbf{Q} = Z = (0, 0, \pi)$ , relevant for  $\text{U}_2\text{Rh}_2\text{Sn}$ [57],  $\text{U}_2\text{Ni}_2\text{In}$ [58], and  $\text{Yb}_2\text{Pd}_2\text{In}_{0.4}\text{Sn}_{0.6}$ [59], here  $\Gamma_{\mathbf{Q}} \otimes_A \Gamma_{\mathbf{Q}} = A_{2g}$ . Since orbital angular momentum  $L_z \in A_{2g}$ ,  $\mathbf{S}_1 \times \mathbf{S}_2 // \hat{z}$  is then a nonrelativistic variant of Ising SOC  $L_z S_z$ . In  $D_{4h}$ ,  $\{x, y\} \in E_u$  and  $\{z\} \in A_{2u}$ . Since  $E_u \otimes_A E_u = A_{2g}$ , the coplanar AFM generates the nonrelativistic antisymmetric spin Hall conductivity  $\sigma_{xy}^z = -\sigma_{yx}^z$ , the same as that from an Ising SOC.

As a second example, consider again space group 127 but with wavevector  $\mathbf{Q} = A = (\pi, \pi, \pi)$ , relevant for  $\text{BaNd}_2\text{PtO}_5$ [60]. Here  $\Gamma_{\mathbf{Q}} \otimes_A \Gamma_{\mathbf{Q}} = A_{1g}$ . Since none of the orbital angular momenta belong to  $A_{1g}$ ,  $\mathbf{S}_1 \times \mathbf{S}_2$  is different from the above Ising SOC, and cannot host anomalous spin Hall conductivities. Instead, it describes a spin-active ferroaxial order, which allows symmetric spin conductivities. Since  $E_u \otimes_S E_u = A_{2g} \otimes A_{2g} = A_{1g}$ , spin conductivities  $\sigma_{xx}^l = \sigma_{yy}^l \neq \sigma_{zz}^l$  are non-zero. Notably, the spin conductivity is pure longitudinal, without transverse Hall components in the non-relativistic limit.

*Microscopic analysis:* While our symmetry arguments imply the existence of non-relativistic spin conductivities, microscopic models are needed to verify that these can be large. To verify this, we carry out a two-prong approach: i) initially develop a minimal models for  $Q = (\pi, \pi, \pi)$  in SG 127 for which a pure longitudinal spin conductivity is predicted (this model can be generalized to many other  $(P, T) = (+, +)$  spin-active magnets) and ii) carry out first principles calculations for the  $(P, T) = (+, +)$  spin-active magnet  $\text{U}_2\text{Ni}_2\text{In}$  in which a nonrelativistic spin Hall effect predicted. Here we consider a minimal model for AFM order with wavevector  $A = (\pi, \pi, \pi)$  in SG127, which describes  $\text{BaNd}_2\text{PtO}_5$ . We consider  $s$ -orbitals on Wyckoff position 2c, with atoms located at  $(0, 1/2, 1/2)$  and  $(1/2, 0, 1/2)$ . The Hamiltonian takes the form

$$\begin{aligned}
H &= \begin{pmatrix} h_0(\mathbf{k}) & O_M \\ O_M^\dagger & \widetilde{h}_0(\mathbf{k} + \mathbf{Q}) \end{pmatrix} \\
&= \begin{pmatrix} \epsilon_0 + t_0 + t_x \tau_x + t_z \tau_z & \mathbf{J}_1 \cdot \vec{\sigma} + \tau_z \mathbf{J}_2 \cdot \vec{\sigma} \\ \mathbf{J}_1 \cdot \vec{\sigma} + \tau_z \mathbf{J}_2 \cdot \vec{\sigma} & \epsilon_0 - t_0 + \widetilde{t}_x \tau_x + \widetilde{t}_z \tau_z \end{pmatrix} \tag{2}
\end{aligned}$$

$\tau_i$  are Pauli matrices for the sublattice degrees of freedom. As in the usual SDW theory[61], the first block  $h_0(\mathbf{k})$  is the nonmagnetic Hamiltonian.  $\widetilde{h}_0(\mathbf{k} + \mathbf{Q})$  is obtained from  $h_0(\mathbf{k})$  by shifting hopping coefficients, considering the Bloch phase factor. The coplanar AFM state is taken as  $(\mathbf{J}_1, \mathbf{J}_2) = (\frac{\mathbf{S}_1 + \mathbf{S}_2}{2}, \frac{\mathbf{S}_1 - \mathbf{S}_2}{2}) = S(\hat{x}, \hat{y})$ . We take time-reversal and inversion operators to be  $T = i\sigma_y K$  and  $P = 1$  (together with  $\mathbf{k} \rightarrow -\mathbf{k}$ ). As described in the SM, this minimal Hamiltonian describes many possible  $(P, T) = (+, +)$  spin active magnets. For SG 127 and Wyckoff 2c, the hopping coefficients are  $t_x = t_{x0} \cos \frac{k_x}{2} \cos \frac{k_y}{2}$ ,  $t_z = t_{z0} \sin k_x \sin k_y$ , and  $\epsilon_0 + t_0 = t_1 (\cos k_x + \cos k_y) - \mu + t_2 \cos k_z$  [62]. For  $\mathbf{Q} = A = (\pi, \pi, \pi)$ , the shifted coefficients in  $\widetilde{h}_0(\mathbf{k} + \mathbf{Q})$  are  $\widetilde{t}_x = t_{x0} \sin \frac{k_x}{2} \sin \frac{k_y}{2}$ ,  $\widetilde{t}_z = t_z$ ,

and  $\epsilon_0 - t_0 = -t_1(\cos k_x + \cos k_y) - \mu - t_2 \cos k_z$ . From our earlier group theory analysis,  $\mathbf{S}_1 \times \mathbf{S}_2$  transforms as  $A_{1g}$  under real-space symmetries, leading to a nonrelativistic, pure longitudinal spin conductivity  $\sigma_{xx}^l = \sigma_{yy}^l$ , as verified in Fig.3 where we have applied a standard Kubo formula (See SI) to calculate these conductivities. Figure 3 also reveals that for a reasonable choice of parameters, it can become appreciable, for example  $\sigma_{xx}^z \approx 300$  ( $\hbar/e$ )S/cm.

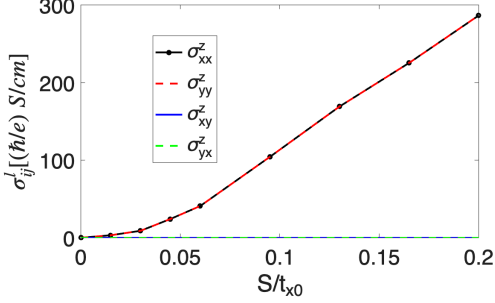


FIG. 3. Spin conductivities for SG127(2c) with wavevector  $A = (\pi, \pi, \pi)$ . Here  $\mathbf{S}_1 \times \mathbf{S}_2$  has  $A_{1g}$  spatial symmetry, giving a longitudinal spin conductivities with  $\sigma_{xx}^l = \sigma_{yy}^l$ . Hopping parameters  $t_{x0} = 1\text{eV}$ ,  $t_{z0} = 0.5t_{x0}$ ,  $t_1 = 0.8t_{x0}$ ,  $t_2 = 0$ , and  $\mu = 0.3t_{x0}$  are used. The lattice constant is  $6\text{\AA}$ . The nonrelativistic spin conductivity is significant for moderately strong spin ordering.

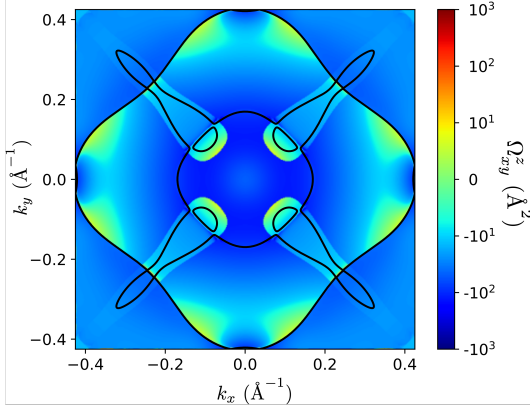


FIG. 4. Nonrelativistic spin Berry curvature of  $\text{U}_2\text{Ni}_2\text{In}$  summed over the occupied bands in the  $k_z = 0$  plane. The solid lines indicate the intersections of the Fermi surface with this plane. The color scale is shown on a logarithmic scale.

We now turn to our DFT calculations of the nonrelativistic spin conductivity in  $\text{U}_2\text{Ni}_2\text{In}$ . Details of the calculations are described in the Supplementary Material. This compound crystallizes in the nonmagnetic space group  $P4/\text{mbm}$  (No. 127) and is known to host a coplanar AFM spin order lying within the  $xy$  plane, with wave vector  $\mathbf{Q} = (0, 0, \pi)$  [63]. Our symmetry analysis predicts a non-zero nonrelativistic spin Hall conductivity for  $\sigma_{xy}^z = -\sigma_{yx}^z$ . As shown in Fig.4, the DFT results for

the spin Berry curvature agree with the symmetry prediction. Here, we defined the spin Berry curvature  $\Omega_{ij}^l$  as

$$\Omega_{ij}^l(\mathbf{k}) = -2 \text{Im} \sum_{m,n} \frac{1}{(E_m - E_n)^2} \times [\langle m | \partial H / \partial k_i | n \rangle \langle n | \{ \partial H / \partial k_j, \hat{\sigma}_l / 2 \} | m \rangle - (i \leftrightarrow j)], \quad (3)$$

where  $|m, n\rangle$  are eigenstates of  $H(\mathbf{k})$ . Notably, the magnitude of the peak spin Berry curvature is comparable to that of Pt[64]. From these calculations, we find a substantial nonrelativistic spin Hall conductivity arising from the  $(P, T) = (+, +)$  state, with  $\sigma_{xy}^z = -\sigma_{yx}^z = -191.1$  ( $\hbar/e$ )S/cm. In contrast, all other nonrelativistic spin Hall components vanish,  $\sigma_{yz}^x = \sigma_{xz}^y = 0$ , in agreement with the symmetry analysis. When SOC is included, the spin Hall conductivities become  $\sigma_{xy}^z = -\sigma_{yx}^z = -417.7$  ( $\hbar/e$ )S/cm. We find that approximately 46% of the spin Hall conductivity,  $\sigma_{xy}^z = -\sigma_{yx}^z$ , arises from nonrelativistic contributions, despite the strong SOC in uranium.

*Circularly polarized light:* While  $(P, T) = (+, +)$  spin-active magnets exhibit no spin splitting, here we show that such a spin-splitting can be generated by circularly polarized light (CPL). CPL coupled to PT-symmetric magnet  $(P, T) = (-, -)$  can unlock odd-parity spin splittings[36–39]. In this section, we will analyze  $(P, T) = (+, +)$  magnets under CPL, and we will illustrate the generation of even-parity ferromagnetic or altermagnetic spin splittings.

CPL is described by a time-dependent vector potential  $\vec{A} = (A_0 \sin \omega t, A_0 \cos \omega t, 0)$ . The symmetry breaking of CPL can be captured by the time-independent T-odd polarization  $\vec{A} \times \partial_t \vec{A}$ . Here,  $\vec{A}$  is a polar vector  $A_i \in \Gamma_V \otimes \Gamma_1^S$  ( $\Gamma_1^S$  denotes a spin-scalar). The cross product transforms as  $\vec{A} \times \partial_t \vec{A} \in (\Gamma_V \otimes_A \Gamma_V) \otimes \Gamma_1^S$ . When acting on  $(P, T) = (+, +)$  magnet, the CPL can induce an even-parity spin splitting  $\mathbf{M}$ , through the trilinear symmetry-allowed coupling  $(\vec{A} \times \partial_t \vec{A}) \mathbf{M} \cdot (\mathbf{S}_1 \times \mathbf{S}_2)$ . This trilinear term requires  $\mathbf{M}$  to be T-odd, transforming as  $\Gamma_M \otimes \Gamma_A^S$  with  $\Gamma_M \subset (\Gamma_V \otimes_A \Gamma_V) \otimes (\Gamma_Q \otimes_A \Gamma_Q)$ , and  $\mathbf{M} / \mathbf{S}_1 \times \mathbf{S}_2$ . The spin splitting is proportional to  $S^2 A_0^2$ .

The CPL-induced spin splitting can be either ferromagnetic or altermagnetic. For example, in tetragonal  $D_{4h}$ , in-plane polar vectors satisfy  $(A_x, A_y) \in E_u$ . The antisymmetric product  $\vec{A} \times \partial_t \vec{A}$  then transforms as  $(E_u \otimes_A E_u) \otimes \Gamma_1^S = A_{2g} \otimes \Gamma_1^S$ . The CPL unlocks a spin-splitting for coplanar AFM at 127Z (e.g.  $\text{U}_2\text{Ni}_2\text{In}$ ) as  $\Gamma_M = A_{2g} \otimes A_{2g} = A_{1g}$ , giving a ferromagnet. The spin-splitting for AFM at 127A (e.g.  $\text{BaNd}_2\text{PtO}_5$ ) is  $\Gamma_M = A_{2g} \otimes A_{1g} = A_{2g} \sim k_x k_y (k_x^2 - k_y^2)$ , giving a g-wave altermagnet. These symmetry arguments are supported by our microscopic Floquet theory using the minimal model introduced in Eq. 2 and can be found in SI.

*Parity symmetry breaking:* Ferroelectricity, electric

fields, and surfaces coupled to PT-symmetric magnet  $(P, T) = (-, -)$  can unlock even-parity ferromagnetic or altermagnetic spin splittings[29]. In this section, we will analyze  $(P, T) = (+, +)$  magnets under an electric field, and we will illustrate the generation of odd-parity spin splittings.

Electric field  $\vec{E}$  is a T-even polar vector  $E_i \in \Gamma_V \otimes \Gamma_1^S$ . When acting on  $(P, T) = (+, +)$  magnet, the electric field can induce an odd-parity spin splitting  $\mathbf{N}_i$ , through the trilinear coupling  $E_i \mathbf{N}_i \cdot (\mathbf{S}_1 \times \mathbf{S}_2)$  in Landau theory. This trilinear term requires  $\mathbf{N}_i$  to be T-even, transforming as  $\Gamma_N \otimes \Gamma_A^S$  with  $\Gamma_N \subset \Gamma_V \otimes (\Gamma_Q \otimes_A \Gamma_Q)$ , and  $\mathbf{N} // \mathbf{S}_1 \times \mathbf{S}_2$ .

For example, in tetragonal system  $D_{4h}$ , out-of-plane electric field satisfies  $E_z \in A_{2u}$ . It unlocks spin splitting for coplanar AFM at 127Z with  $\Gamma_N = A_{2u} \otimes A_{2g} = A_{1u} \sim k_x k_y k_z (k_x^2 - k_y^2)$ , giving a h-wave magnet. The spin splitting for AFM at 127A is  $\Gamma_N = A_{2u} \otimes A_{1g} = A_{2u} \sim k_z$ , giving a p-wave magnet.

*Conclusions:* We have developed a group-theory-based framework for generating  $(P, T) = (+, +)$  spin-active magnets from coplanar antiferromagnets. We constructed 166 phenomenological cases of period-doubling AFM that allow such a state and provided minimal microscopic models for some of these. Our analysis reveals the existence of non-relativistic spin conductivities in the co-planar AFM state. Our microscopic models and DFT calculations on  $U_2Ni_2In$  reveal that these spin conductivities are appreciable. We further demonstrated that circularly polarized light can induce even-parity ferromagnetic or altermagnetic spin splittings, while parity-breaking fields, such as electric fields, can generate odd-parity spin splittings. Our theory is applicable to 16 AFM materials in Magdata database, offering a general framework for spintronics applications in realistic systems.

- 
- [1] Satoru Hayami, Yuki Yanagi, and Hiroaki Kusunose, “Momentum-dependent spin splitting by collinear antiferromagnetic ordering,” *Journal of the Physical Society of Japan* **88**, 123702 (2019).
- [2] Lin-Ding Yuan, Zhi Wang, Jun-Wei Luo, Emmanuel I Rashba, and Alex Zunger, “Giant momentum-dependent spin splitting in centrosymmetric low-z antiferromagnets,” *Physical Review B* **102**, 014422 (2020).
- [3] Igor I Mazin, Klaus Koepf, Michelle D Johannes, Rafael González-Hernández, and Libor Šmejkal, “Prediction of unconventional magnetism in doped fcsb2,” *Proceedings of the National Academy of Sciences* **118**, e2108924118 (2021).
- [4] Libor Šmejkal, Jairo Sinova, and Tomas Jungwirth, “Beyond conventional ferromagnetism and antiferromagnetism: A phase with nonrelativistic spin and crystal rotation symmetry,” *Physical Review X* **12**, 031042 (2022).
- [5] Libor Šmejkal, Jairo Sinova, and Tomas Jungwirth, “Emerging research landscape of altermagnetism,” *Physical Review X* **12**, 040501 (2022).
- [6] J Krempaský, L Šmejkal, SW D’souza, M Hajlaoui, G Springholz, K Uhlířová, F Alarab, PC Constantinou, V Strocov, D Usanov, et al., “Altermagnetic lifting of kramers spin degeneracy,” *Nature* **626**, 517–522 (2024).
- [7] Rafael González-Hernández, Libor Šmejkal, Karel Vyborný, Yuta Yahagi, Jairo Sinova, Tomáš Jungwirth, and Jakub Železný, “Efficient electrical spin splitter based on nonrelativistic collinear antiferromagnetism,” *Physical Review Letters* **126**, 127701 (2021).
- [8] Lei Han, Xizhi Fu, Rui Peng, Xingkai Cheng, Jiankun Dai, Liangyang Liu, Yidian Li, Yichi Zhang, Wenxuan Zhu, Hua Bai, et al., “Electrical 180 switching of néel vector in spin-splitting antiferromagnet,” *Science Advances* **10**, eadn0479 (2024).
- [9] Qirui Cui, Bowen Zeng, Ping Cui, Tao Yu, and Hongxin Yang, “Efficient spin seebeck and spin nernst effects of magnons in altermagnets,” *Physical Review B* **108**, L180401 (2023).
- [10] Libor Šmejkal, Rafael González-Hernández, Tomáš Jungwirth, and Jairo Sinova, “Crystal time-reversal symmetry breaking and spontaneous hall effect in collinear antiferromagnets,” *Science advances* **6**, eaaz8809 (2020).
- [11] Mercè Roig, Yue Yu, Rune C. Ekman, Andreas Kreisel, Brian M. Andersen, and Daniel F. Agterberg, “Quasisymmetry-constrained spin ferromagnetism in altermagnets,” *Physical Review Letters* **135** (2025), 10.1103/839n-rckn.
- [12] Yi Jiang, Ziyin Song, Tiannian Zhu, Zhong Fang, Hongming Weng, Zheng-Xin Liu, Jian Yang, and Chen Fang, “Enumeration of spin-space groups: Toward a complete description of symmetries of magnetic orders,” *Physical Review X* **14**, 031039 (2024).
- [13] Zhenyu Xiao, Jianzhou Zhao, Yanqi Li, Ryuichi Shindou, and Zhi-Da Song, “Spin space groups: Full classification and applications,” *Physical Review X* **14**, 031037 (2024).
- [14] Xiaobing Chen, Jun Ren, Yanzhou Zhu, Yutong Yu, Ao Zhang, Pengfei Liu, Jiayu Li, Yuntian Liu, Caiheng Li, and Qihang Liu, “Enumeration and representation theory of spin space groups,” *Physical Review X* **14**, 031038 (2024).
- [15] Hikaru Watanabe, Kohei Shinohara, Takuya Nomoto, Atsushi Togo, and Ryotaro Arita, “Symmetry analysis with spin crystallographic groups: Disentangling effects free of spin-orbit coupling in emergent electromagnetism,” *Physical Review B* **109**, 094438 (2024).
- [16] Anna Birk Hellenes, Tomáš Jungwirth, Rodrigo Jaeschke-Ubiergo, Atasi Chakraborty, Jairo Sinova, and Libor Šmejkal, “P-wave magnets,” *arXiv preprint arXiv:2309.01607* (2023).
- [17] Jin Matsuda, Hikaru Watanabe, and Ryotaro Arita, “Multiferroic collinear antiferromagnets with hidden altermagnetic spin splitting,” *Physical Review Letters* **134** (2025), 10.1103/vgcs-bn8g.
- [18] Bjørnulf Brekke, Pavlo Sukhachov, Hans Gløckner Giil, Arne Brataas, and Jacob Linder, “Minimal models and transport properties of unconventional p-wave magnets,” *Physical Review Letters* **133**, 236703 (2024).
- [19] Yue Yu, Magnus B Lyngby, Tatsuya Shishidou, Mercè Roig, Andreas Kreisel, Michael Weinert, Brian M Andersen, and Daniel F Agterberg, “Odd-parity magnetism driven by antiferromagnetic exchange,” *Physical Review Letters* **135**, 046701 (2025).
- [20] Xun-Jiang Luo, Jin-Xin Hu, and KT Law, “Spin sym-

- metry criteria for odd-parity magnets,” arXiv preprint arXiv:2510.05512 (2025).
- [21] Aurelien Manchon, Hyun Cheol Koo, Junsaku Nitta, Sergey M Frolov, and Rembert A Duine, “New perspectives for rashba spin-orbit coupling,” *Nature materials* **14**, 871–882 (2015).
- [22] Rafael González-Hernández, Philipp Ritzinger, Karel Vybourný, Jakub Železný, and Aurélien Manchon, “Non-relativistic torque and edelstein effect in non-collinear magnets,” *Nature Communications* **15**, 7663 (2024).
- [23] Mengli Hu, Oleg Janson, Claudia Felser, Paul McClarty, Jeroen van den Brink, and Maia G. Vergniory, “Spin hall and edelstein effects in chiral non-collinear altermagnets,” *Nature Communications* **16**, 8529 (2025).
- [24] Atasi Chakraborty, Anna Birk Hellenes, Rodrigo Jaeschke-Ubiergo, Tomás Jungwirth, Libor Šmejkal, and Jairo Sinova, “Highly efficient non-relativistic edelstein effect in nodal p-wave magnets,” *Nature Communications* **16**, 7270 (2025).
- [25] Hikaru Watanabe and Youichi Yanase, “Nonlinear electric transport in odd-parity magnetic multipole systems: Application to mn-based compounds,” *Physical Review Research* **2**, 043081 (2020).
- [26] Hikaru Watanabe and Youichi Yanase, “Magnetic parity violation and parity-time-reversal-symmetric magnets,” *Journal of Physics: Condensed Matter* **36**, 373001 (2024).
- [27] Satoru Hayami, Megumi Yatsushiro, and Hiroaki Kusunose, “Nonlinear spin hall effect in pt-symmetric collinear magnets,” *Physical Review B* **106**, 024405 (2022).
- [28] Xiuwen Zhang, Qihang Liu, Jun-Wei Luo, Arthur J Freeman, and Alex Zunger, “Hidden spin polarization in inversion-symmetric bulk crystals,” *Nature Physics* **10**, 387–393 (2014).
- [29] Igor Mazin, Rafael González-Hernández, and Libor Šmejkal, “Induced monolayer altermagnetism in mnp (s, se)  $_3$  and fese,” arXiv preprint arXiv:2309.02355 (2023).
- [30] Dinghui Wang, Huaiqiang Wang, Lulu Liu, Juntong Zhang, and Haijun Zhang, “Electric-field-induced switchable two-dimensional altermagnets,” *Nano Letters* **25**, 498–503 (2024).
- [31] Mingqiang Gu, Yuntian Liu, Haiyuan Zhu, Kunihiro Yananose, Xiaobing Chen, Yongkang Hu, Alessandro Stroppa, and Qihang Liu, “Ferroelectric switchable altermagnetism,” *Physical Review Letters* **134**, 106802 (2025).
- [32] Wei Sun, Changhong Yang, Wenxuan Wang, Ying Liu, Xiaotian Wang, Shifeng Huang, and Zhenxiang Cheng, “Proposing Altermagnetic-Ferroelectric Type-III Multiferroics with Robust Magnetoelectric Coupling,” *Advanced Materials* **37**, 2502575 (2025).
- [33] Himanshu Mavani, Kai Huang, Kartik Samanta, and Evgeny Y Tsybal, “Two-dimensional antiferromagnets with nonrelativistic spin splitting switchable by electric polarization,” *Physical Review B* **112**, L060401 (2025).
- [34] Libor Šmejkal, “Altermagnetic multiferroics and altermagnetoelectric effect,” (2024), arXiv:2411.19928 [cond-mat.mtrl-sci].
- [35] Xunkai Duan, Jiayong Zhang, Ziye Zhu, Yuntian Liu, Zhenyu Zhang, Igor Žutić, and Tong Zhou, “Antiferroelectric altermagnets: Antiferroelectricity alters magnets,” *Phys. Rev. Lett.* **134**, 106801 (2025).
- [36] P. Zhou, X. N. Peng, Y. Z. Hu, B. R. Pan, S. M. Liu, P. B. Lyu, and L. Z. Sun, “Transition from antiferromagnets to altermagnets: Symmetry-breaking theory,” *Physical Review B* **112**, 144419 (2025).
- [37] Tongshuai Zhu, Di Zhou, Huaiqiang Wang, and Jiawei Ruan, “Floquet odd-parity collinear magnets,” arXiv preprint arXiv:2508.02542 (2025).
- [38] Bo Li, Ding-Fu Shao, and Alexey A Kovalev, “Floquet spin splitting and spin generation in antiferromagnets,” arXiv preprint arXiv:2507.22884 (2025).
- [39] Shengpu Huang, Zheng Qin, Fangyang Zhan, Dong-Hui Xu, Da-Shuai Ma, and Rui Wang, “Light-induced odd-parity magnetism in conventional collinear antiferromagnets,” arXiv preprint arXiv:2507.20705 (2025).
- [40] Mikhail I Dyakonov, “Possibility of orienting electron spins with current,” *JETP Lett. USSR* **13**, 467 (1971).
- [41] Jairo Sinova, Sergio O Valenzuela, Jörg Wunderlich, Craig H Back, and Tomáš Jungwirth, “Spin hall effects,” *Reviews of modern physics* **87**, 1213–1260 (2015).
- [42] Yuichiro K Kato, Roberto C Myers, Arthur C Gossard, and David D Awschalom, “Observation of the spin hall effect in semiconductors,” *science* **306**, 1910–1913 (2004).
- [43] Satoru Hayami, Rikuto Oiwa, and Hiroaki Kusunose, “Electric ferro-axial moment as nanometric rotator and source of longitudinal spin current,” *Journal of the Physical Society of Japan* **91**, 113702 (2022).
- [44] Yang Zhang, Jakub Železný, Yan Sun, Jeroen van den Brink, and Binghai Yan, “Spin hall effect emerging from a noncollinear magnetic lattice without spin-orbit coupling,” *New Journal of Physics* **20**, 073028 (2018).
- [45] Yang Zhang, Yan Sun, Hao Yang, Jakub Železný, Stuart P. P. Parkin, Claudia Felser, and Binghai Yan, “Strong anisotropic anomalous Hall effect and spin Hall effect in the chiral antiferromagnetic compounds  $mn_3x$  ( $x = Ge, Sn, Ga, Ir, Rh, \text{ and } Pt$ ),” *Phys. Rev. B* **95**, 075128 (2017).
- [46] Makoto Naka, Satoru Hayami, Hiroaki Kusunose, Yuki Yanagi, Yukitoshi Motome, and Hitoshi Seo, “Spin current generation in organic antiferromagnets,” *Nature Communications* **10**, 4305 (2019).
- [47] Kyo-Hoon Ahn, Atsushi Hariki, Kwan-Woo Lee, and Jan Kuneš, “Antiferromagnetism in  $RuO_2$  as d-wave Pomeranchuk instability,” *Physical Review B* **99**, 184432 (2019).
- [48] Hai-Yang Ma, Mengli Hu, Nana Li, Jianpeng Liu, Wang Yao, Jin-Feng Jia, and Junwei Liu, “Multifunctional antiferromagnetic materials with giant piezomagnetism and noncollinear spin current,” *Nature Communications* **12**, 2846 (2021).
- [49] Rafael González-Hernández, Libor Šmejkal, Karel Vybourný, Yuta Yahagi, Jairo Sinova, Tomáš Jungwirth, and Jakub Železný, “Efficient electrical spin splitter based on nonrelativistic collinear antiferromagnetism,” *Physical Review Letters* **126**, 127701 (2021).
- [50] Frank Freimuth, Stefan Blügel, and Yuriy Mokrousov, “Spin-orbit torques in co/pt(111) and mn/w(001) magnetic bilayers from first principles,” *Phys. Rev. B* **90**, 174423 (2014).
- [51] J. Železný, H. Gao, Aurélien Manchon, Frank Freimuth, Yuriy Mokrousov, J. Zemen, J. Mašek, Jairo Sinova, and T. Jungwirth, “Spin-orbit torques in locally and globally noncentrosymmetric crystals: Antiferromagnets and ferromagnets,” *Phys. Rev. B* **95**, 014403 (2017).
- [52] Hikaru Watanabe, Yue Yu, Jin Matsuda, Daniel Agterberg, and Ryotaro Arita, “Ferroaxial magnets: timereversal- and mirror symmetry violation from spin order,” arXiv preprint arXiv: (2026).

- [53] Luis Elcoro, Barry Bradlyn, Zhijun Wang, Maia G Vergniory, Jennifer Cano, Claudia Felser, B Andrei Bernevig, Danel Orobengoa, G Flor, and Mois I Aroyo, “Double crystallographic groups and their representations on the Bilbao crystallographic server,” *Applied Crystallography* **50**, 1457–1477 (2017).
- [54] Paul A. McClarty and Jeffrey G. Rau, “Landau Theory of Altermagnetism,” *Phys. Rev. Lett.* **132**, 176702 (2024).
- [55] Rikuto Oiwa and Hiroaki Kusunose, “Systematic analysis method for nonlinear response tensors,” *Journal of the Physical Society of Japan* **91**, 014701 (2022).
- [56] Samuel V Gallego, J Manuel Perez-Mato, Luis Elcoro, Emre S Tasci, Robert M Hanson, Koichi Momma, Mois I Aroyo, and Gotzon Madariaga, “Magndata: towards a database of magnetic structures. i. the commensurate case,” *Applied Crystallography* **49**, 1750–1776 (2016).
- [57] K Prokeš, DI Gorbunov, M Reehuis, B Klemke, A Gukasov, K Uhlířová, X Fabrèges, Y Skourski, F Yokaichiya, S Hartwig, et al., “Anisotropic physical properties of single-crystal  $\text{U}_2\text{Rh}_2\text{Sn}$  in high magnetic fields,” *Physical Review B* **95**, 174433 (2017).
- [58] Heinz Nakotte, A Purwanto, RA Robinson, Karel Prokes, JCP Klaasse, PF De Chatel, Frank R de Boer, Ladislav Havela, V Sechovský, Laura CJ Pereira, et al., “Hybridization effects in  $\text{U}_2\text{T}_2\text{X}$  compounds: Magnetic structures of  $\text{U}_2\text{Rh}_2\text{Sn}$  and  $\text{U}_2\text{Ni}_2\text{In}$ ,” *Physical Review B* **53**, 3263 (1996).
- [59] A Martinelli, S Sanna, G Lamura, C Ritter, B Joseph, E Bauer, and M Giovannini, “Structural and magnetic properties of the  $\text{Yb}_2\text{Pd}_2(\text{In}_{1-x}\text{Sn}_x)$  system: a synchrotron x-ray and neutron powder diffraction investigation,” *Journal of Physics: Condensed Matter* **31**, 385802 (2019).
- [60] Christopher M Pasco, Binod K Rai, Matthias Frontzek, Gabriele Sala, Matthew B Stone, Bryan C Chakoumakos, V Ovidiu Garlea, Andrew D Christianson, and Andrew F May, “Anisotropic magnetism of the Shastry-Sutherland lattice material  $\text{BaNd}_2\text{PtO}_5$ ,” *Physical Review Materials* **7**, 074407 (2023).
- [61] Assa Auerbach, *Interacting electrons and quantum magnetism* (Springer Science & Business Media, 2012).
- [62] Mercè Roig, Andreas Kreisler, Yue Yu, Brian M Andersen, and Daniel F Agterberg, “Minimal models for altermagnetism,” *Physical Review B* **110**, 144412 (2024).
- [63] A. Martin-Martin, L. C. J. Pereira, G. H. Lander, J. Rebizant, F. Wastin, J. C. Spirlet, P. Dervenagas, and P. J. Brown, “Neutron-diffraction studies of single crystals of  $\text{U}_2\text{T}_2\text{In}$  ( $T = \text{Ni, Pd, Pt}$ ),” *Physical Review B* **59**, 11818–11825 (1999).
- [64] Junfeng Qiao, Jiaqi Zhou, Zhe Yuan, and Weisheng Zhao, “Calculation of intrinsic spin Hall conductivity by Wannier interpolation,” *Physical Review B* **98**, 214402 (2018).
- [65] RM Fernandes, SA Kivelson, and Erez Berg, “Vestigial chiral and charge orders from bidirectional spin-density waves: Application to the iron-based superconductors,” *Physical Review B* **93**, 014511 (2016).
- [66] G. Kresse and J. Furthmüller, “Efficient iterative schemes for ab initio total-energy calculations using a plane-wave basis set,” *Physical Review B* **54**, 11169–11186 (1996).
- [67] John P. Perdew, Kieron Burke, and Matthias Ernzerhof, “Generalized Gradient Approximation Made Simple,” *Physical Review Letters* **77**, 3865–3868 (1996).
- [68] P. E. Blöchl, “Projector augmented-wave method,” *Physical Review B* **50**, 17953–17979 (1994).
- [69] Nicola Marzari and David Vanderbilt, “Maximally localized generalized Wannier functions for composite energy bands,” *Physical Review B* **56**, 12847–12865 (1997).
- [70] Ivo Souza, Nicola Marzari, and David Vanderbilt, “Maximally localized Wannier functions for entangled energy bands,” *Physical Review B* **65**, 035109 (2001).
- [71] Giovanni Pizzi, Valerio Vitale, Ryotaro Arita, Stefan Blügel, Frank Freimuth, Guillaume Géranton, Marco Gibertini, Dominik Gresch, Charles Johnson, Takashi Koretsune, Julen Ibañez-Azpiroz, Hyungjun Lee, Jae-Mo Lihm, Daniel Marchand, Antimo Marrazzo, Yuriy Mokrousov, Jamal I Mustafa, Yoshiro Nohara, Yusuke Nomura, Lorenzo Paulatto, Samuel Poncé, Thomas Ponweiser, Junfeng Qiao, Florian Thöle, Stepan S Tsirkin, Małgorzata Wierzbowska, Nicola Marzari, David Vanderbilt, Ivo Souza, Arash A Mostofi, and Jonathan R Yates, “Wannier90 as a community code: new features and applications,” *Journal of Physics: Condensed Matter* **32**, 165902 (2020).
- [72] Wahyu Setyawan and Stefano Curtarolo, “High-throughput electronic band structure calculations: Challenges and tools,” *Computational Materials Science* **49**, 299 (2010).
- [73] Wei Wang, Nan Xu, Jin-Cheng Liu, Gang Tang, and Wen-Tong Geng, “VASPKIT: A user-friendly interface facilitating high-throughput computing and analysis using VASP code,” *Computer Physics Communications* **267**, 108033 (2021).
- [74] Stepan S Tsirkin, “High performance Wannier interpolation of Berry curvature and related quantities with WannierBerri code,” *npj computational materials* **7**, 1 (2021).
- [75] Mark S Rudner and Netanel H Lindner, “Band structure engineering and non-equilibrium dynamics in floquet topological insulators,” *Nature Reviews Physics* **2**, 229–244 (2020).
- [76] Takuya Kitagawa, Takashi Oka, Arne Brataas, Liang Fu, and Eugene Demler, “Transport properties of nonequilibrium systems under the application of light: Photoinduced quantum Hall insulators without Landau levels,” *Physical Review B* **84**, 235108 (2011).
- [77] Nathan Goldman and Jean Dalibard, “Periodically driven quantum systems: Effective hamiltonians and engineered gauge fields,” *Physical review X* **4**, 031027 (2014).
- [78] Takahiro Mikami, Sota Kitamura, Kenji Yasuda, Naoto Tsuji, Takashi Oka, and Hideo Aoki, “Brillouin-wigner theory for high-frequency expansion in periodically driven systems: Application to floquet topological insulators,” *Physical Review B* **93**, 144307 (2016).
- [79] Marin Bukov, Luca D’Alessio, and Anatoli Polkovnikov, “Universal high-frequency behavior of periodically driven systems: from dynamical stabilization to floquet engineering,” *Advances in Physics* **64**, 139–226 (2015).
- [80] André Eckardt and Egidijus Anisimovas, “High-frequency approximation for periodically driven quantum systems from a floquet-space perspective,” *New journal of physics* **17**, 093039 (2015).

## ACKNOWLEDGEMENT

D.F.A. and Y.Y. were supported by the Department of Energy, Office of Basic Energy Science, Division of Materials Sciences and Engineering under Award No DE-SC0021971. This work is supported by Grant-in-Aid for Scientific Research from JSPS KAKENHI Grant No. JP23K13058 (H.W.), No. JP24K00581 (H.W.), No. JP25H02115 (H.W.), No. JP21H04990 (R.A.), No. JP25H01246 (R.A.), No. JP25H01252 (R.A.), JST-CREST No. JPMJCR23O4(R.A.), JST-ASPIRE No. JPMJAP2317 (R.A.), JST-Mirai No. JPMJMI20A1 (R.A.), and RIKEN TRIP initiative (RIKEN Quantum, Advanced General Intelligence for Science Program, Manybody Electron Systems). H.W. was also supported by JSR Corporation via JSR-UTokyo Collaboration Hub, CURIE.

## END MATTER

Here, we present the phase diagrams for the Landau free energy in Eq.1.

$$\beta_4 = 0, \beta_2 \neq \beta_3$$

The results for  $\beta_4 = 0$  and  $\beta_2 \neq \beta_3$  can be found in [19, 65]. There are three competing phases:  $(\mathbf{S}_1, \mathbf{S}_2) \propto (\hat{x}, \hat{x})$ ,  $(0, \hat{x})$ , and  $(\hat{x}, \hat{y})$ . The phase diagram is shown in Fig.5. The phase boundaries are located at  $\beta_2 = 0$ ,  $\beta_3 = 0$ , and  $\beta_2 = \beta_3$ . The coplanar phase requires  $\beta_{2,3} > 0$ .

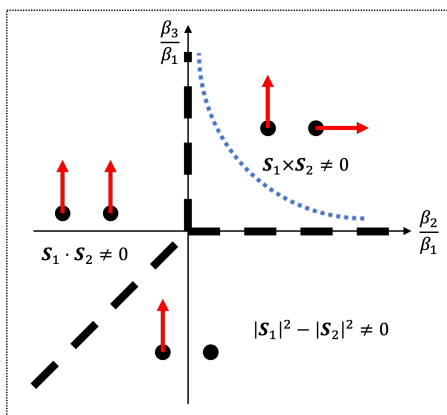


FIG. 5. Phase diagram for  $\beta_4 = 0$  is shown as thick black dashed line. When  $\beta_4 \neq 0$ , the two collinear phases mix up, and the phase boundary between collinear and coplanar phases is at the blue dotted line.

$$\beta_4 \neq 0$$

When all the real-space symmetries take  $(\mathbf{S}_1, \mathbf{S}_2)$  to either  $\pm(\mathbf{S}_1, \mathbf{S}_2)$  or  $\pm(\mathbf{S}_2, -\mathbf{S}_1)$ , inner products  $\mathbf{S}_1 \cdot \mathbf{S}_2$  and  $\mathbf{S}_1 \cdot \mathbf{S}_1 - \mathbf{S}_2 \cdot \mathbf{S}_2$  carry the same symmetry. This allowed  $\beta_4 \neq 0$ , and happens in 64 2D IRs, listed in the middle part of Table.II in SI.

For the phase diagram, we compare solutions with the same  $R \equiv \mathbf{S}_1 \cdot \mathbf{S}_1 + \mathbf{S}_2 \cdot \mathbf{S}_2$ . The energy contributions from the quadratic term and the  $\beta_1$  term are then the same. It is convenient to define  $X \equiv 2\mathbf{S}_1 \cdot \mathbf{S}_2$ , and  $Y \equiv \mathbf{S}_1 \cdot \mathbf{S}_1 - \mathbf{S}_2 \cdot \mathbf{S}_2$ .  $(X, Y)$  belongs to the circle  $X^2 + Y^2 \leq R^2$ . The free energy is  $f = f_0(R) + \beta_2 X^2 + \beta_3 Y^2 + \beta_4 XY$ , where  $f_0$  only depends on  $R$ .

If the energy minimum is located on the boundary of the circle, spin orderings are collinear. We can take  $X = R \cos \theta$  and  $Y = R \sin \theta$ , and the free energy becomes  $f = f_0(R) + R^2(\beta_2 \cos^2 \theta + \beta_3 \sin^2 \theta + \beta_4 \cos \theta \sin \theta)$ . Minimizing the energy gives  $(\cos 2\theta, \sin 2\theta) \propto -(\beta_2 - \beta_3, \beta_4)$ . For generic  $\beta_i$ , the solution is  $(\mathbf{S}_1, \mathbf{S}_2) = (S_1 \hat{x}, S_2 \hat{x})$ , with  $S_1 \neq S_2 \neq 0$ . The free energy is  $f = f_0(R) + R^2 \left[ \frac{\beta_2 + \beta_3}{2} - \sqrt{\left(\frac{\beta_2 - \beta_3}{2}\right)^2 + \left(\frac{\beta_4}{2}\right)^2} \right]$

If the energy minimum is located inside the circle, the solution satisfies  $\partial_X f = \partial_Y f = 0$ . Without fine-tuning, the only solution is  $(X, Y) = (0, 0)$ . This corresponds to the coplanar spin ordering  $(\mathbf{S}_1, \mathbf{S}_2) = S(\hat{x}, \hat{y})$ . The free energy is  $f = f_0(R)$ .

The phase boundary between the collinear and coplanar phases is at  $2\beta_2\beta_3 = \beta_4^2$  with  $\beta_{2,3} > 0$  (blue dotted line in Fig.5). As  $\beta_4 \rightarrow 0$ , the boundary recovers to  $\beta_2 = 0$  and  $\beta_3 = 0$ .

$$\beta_2 = \beta_3$$

When inner products  $2\mathbf{S}_1 \cdot \mathbf{S}_2$  and  $\mathbf{S}_1 \cdot \mathbf{S}_1 - \mathbf{S}_2 \cdot \mathbf{S}_2$  belong to a 2D IR  $E_x$ ,  $\beta_2 = \beta_3 = \beta$ .  $\beta_4$  is zero, since the two inner products transform differently. This happens in 40 2D IRs, listed in the last part of Table.I.

While the phase boundary between the coplanar phase and the two collinear phases remains valid  $\beta_2 = \beta_3 = 0$  (Fig.5), the quartic free energy is insufficient to determine the phase transition into the collinear states.

These 40 scenarios all carry a three-fold rotational symmetry, and  $E_x \otimes_S E_x \otimes_S E_x$  contains the trivial IR. The Landau term formed by  $X \equiv 2\mathbf{S}_1 \cdot \mathbf{S}_2$  and  $Y \equiv \mathbf{S}_1 \cdot \mathbf{S}_1 - \mathbf{S}_2 \cdot \mathbf{S}_2$  resembles those in hexagonal systems. For example, if  $(X, Y)$  transform as  $E_{2g} = \{2xy, x^2 - y^2\}$  in hexagonal system  $D_{6h}$ , the free energy is:

$$f = aR + \beta_1 R^2 + \beta(X^2 + Y^2) + \gamma R(X^2 + Y^2) + uY(Y^2 - 3X^2) \quad (4)$$

We focus on the collinear phases, where  $X^2 + Y^2 = R^2$ .

The free energy simplifies to

$$f = f_1(R) + uY(Y^2 - 3X^2) \quad (5)$$

where  $f_1$  only depends on  $R$ . There are three solutions, describing the spontaneous three-fold rotational symmetry breaking. For  $u > 0$ , the three solutions are  $X = R \cos \theta, Y = R \sin \theta$ , with  $\theta = \pi/6 + 2n\pi/3$ . For  $u < 0$ , the three solutions are  $\theta = -\pi/6 + 2n\pi/3$ .

### Kubo formula for Fig.3

In Fig.3, we apply Kubo formula to compute the 3D spin conductivities:

$$\sigma_{ij}^l = -\frac{\hbar}{e} \times \frac{e^2}{Na\hbar} \text{Im} \sum_{\mathbf{k}} \sum_{m,n} \frac{f(E_m) - f(E_n)}{(E_m - E_n)^2} \langle m | \hat{J}_i | n \rangle \langle n | \hat{J}_j^l | m \rangle \quad (6)$$

Current and spin current operators are  $\hat{J}_i = \partial H / \partial k_i$  and  $\hat{J}_j^l = \frac{1}{2} \{ \partial H / \partial k_j, \sigma_l / 2 \}$ .  $a$  is the lattice constant.  $N = 100^3$  momentum points are sampled.  $f(E) = \theta(-E)$  is the Fermi-Dirac distribution at zero temperature.

### DFT calculations

DFT calculations were performed using the Vienna *ab initio* Simulation Package (VASP)[66]. Projector augmented-wave (PAW) PBE pseudopotentials were employed [67, 68]. The crystal and magnetic structure of  $\text{U}_2\text{Ni}_2\text{In}$  were adopted from Ref. [63]. The Brillouin zone was sampled using a  $\Gamma$ -centered  $6 \times 6 \times 8$  k-point mesh, and the plane-wave energy cutoff was set to 400 eV. The threshold of energy convergence was set to  $10^{-6}$  eV.

Maximally localized Wannier functions were constructed using Wannier90 [69–71]. For the initial projections, we included U-*d*, U-*f*, In-*p*, Ni-*s*, Ni-*p*, and Ni-*d* orbitals. The resulting Wannier Hamiltonian has a dimension of  $360 \times 360$ , including spin degrees of freedom. The band structures computed using the Wannier Hamiltonian are in good agreement with the DFT band structures within the energy range of -6 to 3 eV, as shown in Fig.6.

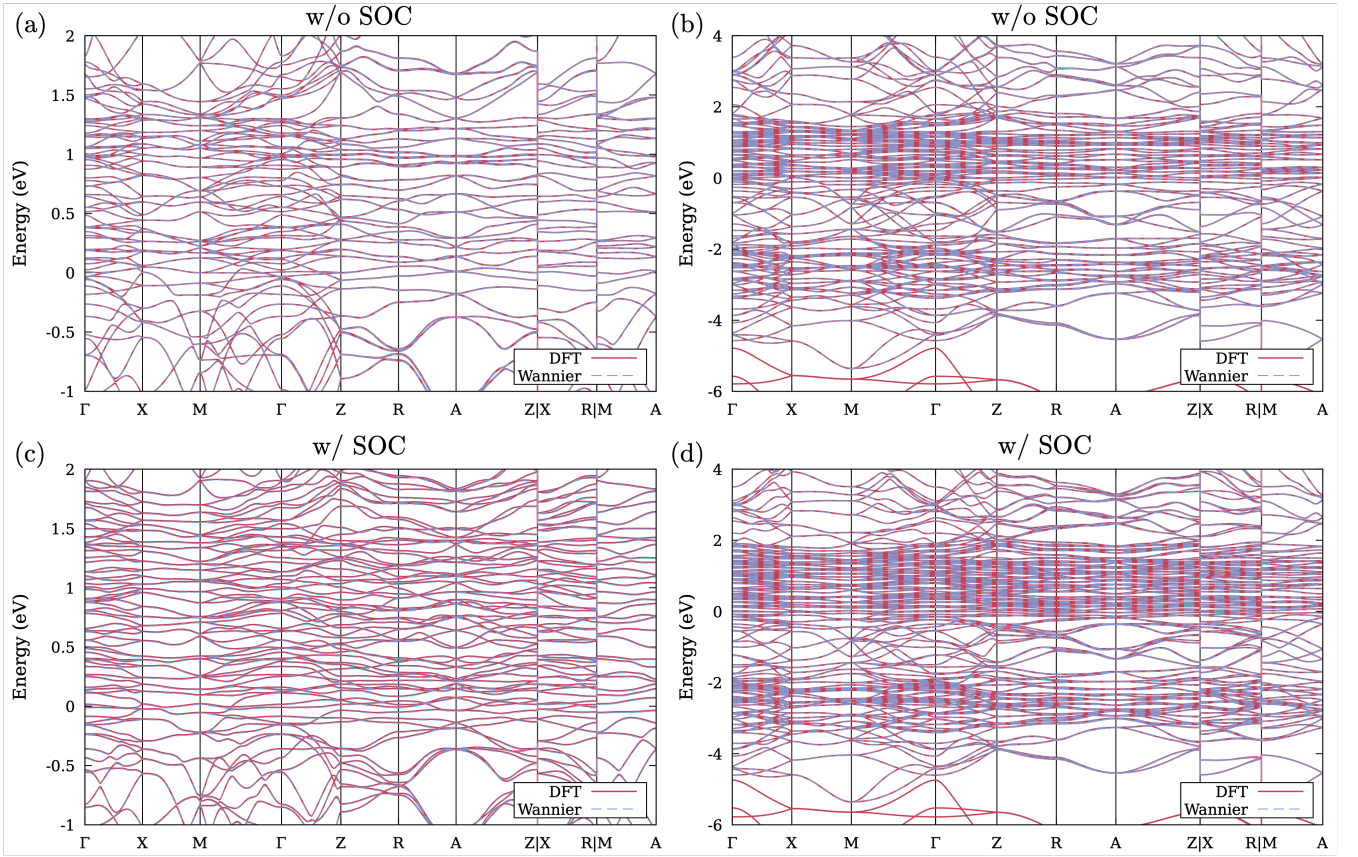


FIG. 6. Band structures of  $\text{U}_2\text{Ni}_2\text{In}$  along the standard high-symmetry path of the Brillouin zone [72]. Red solid (blue dashed) lines represent DFT (Wannier-Hamiltonian) bands. The Fermi energy is set to 0. SOC was excluded in (a), (b) and included in (c), (d). The DFT bands were plotted using VASPKIT [73].

The spin Hall conductivity and spin Berry curvature were evaluated using WANNIERRI [74]. For the Wannier interpolation, the first Brillouin zone was discretized with a  $120 \times 120 \times 160$  mesh. The Wannier interpolation

formalism for the spin Hall conductivity and spin Berry curvature follows Ref. [64]. We plotted the Fermi lines utilizing POSTW90.X code.

The spin Berry curvature summed over the occupied bands along the high-symmetry line is shown in Fig. 7(a). The peak value is approximately approximately  $-400 \text{ \AA}^2$ , which is comparable to those in Pt,  $\alpha$ -Ta and  $\beta$ -Ta [64]. Fig 7 (b) compares the spin Hall conductivities obtained with and without SOC. Without SOC, only  $\sigma_{xy}^z$  and  $\sigma_{yx}^z$  are nonzero, satisfying  $\sigma_{xy}^z = -\sigma_{yx}^z$  in agreement with the symmetry analysis. By contrast, when SOC is included,  $\sigma_{xy}^z = -\sigma_{yx}^z$ ,  $\sigma_{xz}^y = -\sigma_{yz}^x$ , and  $-\sigma_{zx}^y = \sigma_{zy}^x$  become nonzero.

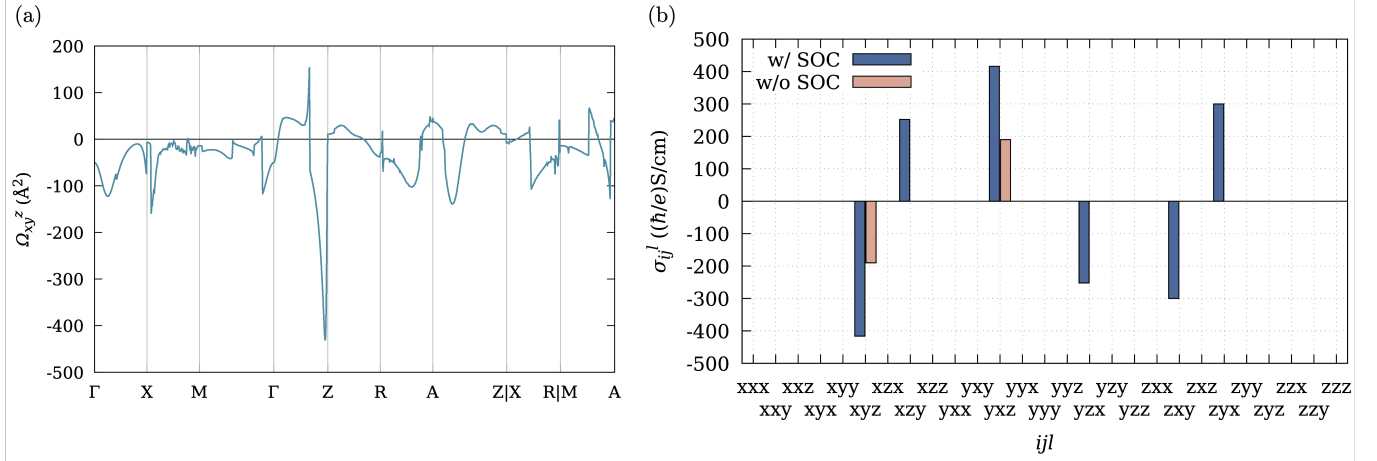


FIG. 7. (b) The spin Hall conductivities with (blue) and without (red) SOC. The horizontal represents the index of spin Hall conductivities.

### Microscopic Floquet theory

Microscopically, CPL leads to a time-dependent Hamiltonian, that can be analyzed using Floquet-Bloch theory[75]. The light is described through Peierls substitution  $H(\mathbf{k}) \rightarrow H(t) = H(\mathbf{k} + \mathbf{A}(t))$ . The eigenstate is expressed by the Floquet-Bloch state  $|\psi(t)\rangle = \exp(-i\varepsilon t)|\phi(t)\rangle$ . The quasi-energy  $\varepsilon$  is well-defined up to  $m\omega$  for integer  $m$ . The Floquet state is periodic  $|\phi(t)\rangle = |\phi(t + 2\pi/\omega)\rangle$ , and satisfies  $(\varepsilon_n + i\partial_t)|\phi(t)\rangle = H(t)|\phi(t)\rangle$ . In frequency space, the eigenvalue equation reads:

$$(\varepsilon + m\omega)|\phi^{(m)}\rangle = \sum_{m'} H^{(m-m')}|\phi^{(m')}\rangle, \quad (7)$$

where  $|\phi^{(m)}\rangle$  and  $H^{(m)}$  is the  $m$ -th Fourier component of the Floquet state and the periodic Hamiltonian.

Fourier components  $h^{(\pm m)}$  contain  $m$ -th order Bessel functions, which scale as  $A_0^m$  for small  $A_0$ . Focusing on the leading components  $h^{(\pm 1)}$ , the effective normal-state Hamiltonian is [76–80]:

$$h_{eff}^{(0)} = h^{(0)} + \frac{[h^{(-1)}, h^{(1)}]}{\omega}. \quad (8)$$

The correction to the normal-state Hamiltonian is from the commutator between  $\tau_x$  and  $\tau_z$ . This results in a  $\tau_y$  term with coefficients  $-2i/\omega(t_x^{(-1)}t_z^{(1)} - t_x^{(1)}t_z^{(-1)})$ . Here,  $t_{x,\mathbf{k}}^{(\pm 1)}$  are the  $\pm 1$  frequency components of  $t_{x,\mathbf{k}+\mathbf{A}(t)}$ . Note that the  $\tau_y$  term is odd under time-reversal symmetry with  $\mathbf{k}$ -even coefficients, consistent with the breaking of this symmetry with CPL.

For SG127 with Wyckoff position  $2c$ ,  $t_{x,z}^{(\pm 1)}$  are:

$$\begin{aligned} t_x^{(1)} &= (t_x^{(-1)})^* = \frac{t_{x0}}{2} J_1\left(\frac{A_0}{\sqrt{2}}\right) e^{-i\pi/4} \left(-i \sin \frac{k_x + k_y}{2} + \sin \frac{k_x - k_y}{2}\right) \\ t_z^{(1)} &= (t_z^{(-1)})^* = \frac{t_{z0}}{2} J_1(\sqrt{2}A_0) e^{-i\pi/4} (i \sin(k_x + k_y) + \sin(k_x - k_y)) \end{aligned} \quad (9)$$

Here  $J_1(x)$  is the first Bessel function. The effective Hamiltonian is

$$h_{eff}^{(0)} = \epsilon_{0,\mathbf{k}}^{(0)} + t_{0,\mathbf{k}}^{(0)} + t_{x,\mathbf{k}}^{(0)}\tau_x + t_{y,\mathbf{k}}\tau_y + t_{z,\mathbf{k}}^{(0)}\tau_z, \quad (10)$$

where zeroth frequency components carry zeroth-order Bessel function, e.g.  $t_x^{(0)} = t_x J_0(A_0/\sqrt{2})$ ,  $t_z^{(0)} = t_z J_0(\sqrt{2}A_0)$ . For small  $A_0$ , these zeroth-order Bessel functions approach 1, and we will neglect them in the following discussion.  $t_{y,\mathbf{k}} = t_{y0} \cos \frac{k_x}{2} \cos \frac{k_y}{2} (\cos k_x - \cos k_y) \in B_{1g}$ , with  $t_{y0} = -2t_{x0}t_{z0}J_1(A_0/\sqrt{2})J_1(A_0\sqrt{2})/\omega$ . For Wyckoff position 127(2c), operators  $\tau_{y,z}$  carries the  $B_{2g}$  site symmetry. The  $t_y\tau_y$  term thus carries  $B_{1g} \otimes B_{2g} = A_{2g}$  symmetry. It is T-odd since  $\tau_y$  is imaginary. For small  $A_0$ ,  $t_{y0}$  scales as  $A_0^2$ . The  $t_y\tau_y$  term thus follows  $\vec{A} \times \partial_t \vec{A}$ .

We include the  $t_y\tau_y$  term in the AFM Hamiltonian to check spin splittings:

$$H_{eff}^{(0)} = \begin{pmatrix} h_0(\mathbf{k}) + t_y\tau_y & O_M \\ O_M^\dagger & \widetilde{h}_0(\mathbf{k} + \mathbf{Q}) + \widetilde{t}_y\tau_y \end{pmatrix} \quad (11)$$

$$\equiv \epsilon_0 + t_1\rho_0\tau_x + t_3\rho_z\tau_x + t_5\rho_0\tau_z + t_6\rho_z\tau_z + t_2\rho_0\tau_y + t_4\rho_z\tau_y + t_0\rho_z + \rho_x(\mathbf{J}_1 \cdot \vec{\sigma} + \tau_z\mathbf{J}_2 \cdot \vec{\sigma}),$$

where  $t_{1,3} \equiv (t_x \pm \widetilde{t}_x)/2$ ,  $t_{2,4} \equiv (t_y \pm \widetilde{t}_y)/2$ , and  $t_{5,6} \equiv (t_z \pm \widetilde{t}_z)/2$ . The dispersion for  $t_0 = 0$  is:

$$E_{\alpha\beta\gamma} = \gamma \left\{ 2S^2 + |\mathbf{t}|^2 + 2\beta[S^2(|\mathbf{t}|^2 + t_5^2 - t_6^2) + 2\alpha S^2(t_1t_4 - t_2t_3) + (t_1t_3 + t_2t_4 + t_5t_6)^2]^{1/2} \right\}^{1/2} \quad (12)$$

Here,  $\alpha, \beta, \gamma = \pm$  and  $|\mathbf{t}|^2 \equiv t_1^2 + t_2^2 + t_3^2 + t_4^2 + t_5^2 + t_6^2$ . The spin splitting depends on  $S^2(t_1t_4 - t_2t_3) \propto S^2(t_y\widetilde{t}_x - t_x\widetilde{t}_y)$ . For 127A,  $\widetilde{t}_y = -t_{y0} \sin \frac{k_x}{2} \sin \frac{k_y}{2} (\cos k_x - \cos k_y)$ , and the spin splitting is proportional to  $S^2 A_0^2 \sin k_x \sin k_y (\cos k_x - \cos k_y)$ . The g-wave spin splitting with magnitude  $S^2 A_0^2$  agrees with the group theory analysis.

TABLE I.  $\Gamma_{\mathbf{Q}} \otimes_{A,S} \Gamma_{\mathbf{Q}}$  for 2D IRs  $\Gamma_{\mathbf{Q}}$  with trivial inversion. The point group keeping TRIM  $\mathbf{Q}$  invariant is included. Antisymmetric direct product  $\Gamma_{\mathbf{Q}} \otimes_A \Gamma_{\mathbf{Q}}$  is put inside the bracket, describing the symmetry breaking from the coplanar state  $\mathbf{S}_1 \times \mathbf{S}_2$ . The first component, e.g.  $A_g$  in  $C_{2h}$ , describes the trivial symmetry breaking of  $\mathbf{S}_1 \cdot \mathbf{S}_1 + \mathbf{S}_2 \cdot \mathbf{S}_2$ . The other components outside the bracket denote the symmetry breaking from the collinear states  $\mathbf{S}_1 \cdot \mathbf{S}_1 - \mathbf{S}_2 \cdot \mathbf{S}_2$  and  $\mathbf{S}_1 \cdot \mathbf{S}_2$ . When number 2 appears, such as in the  $2B_g$  IRs in  $C_{2h}$ , the two collinear states have the same symmetry and belong to the same 1D IR (then  $\beta_4 \neq 0$  in Landau theory). When  $E_x$  IR appears, such as the  $E_g$  IR in  $S_6$ , the two collinear states belong to the same 2D IR (then  $\beta_2 = \beta_3$  in Landau theory).

$D_{2h} : A_g + B_{ig} + B_{jg} + [B_{kg}]$ $i \neq j \neq k$	$52(T_{1+,1-}), 53(U_{1+,1-}, R_{1+,1-}),$ $58(U_{1+,1-}, T_{1+,1-}), 60(S_{1+,1-}), 128(R_{1+,1-}), 136(R_{1+,1-})$
$D_{4h} : A_{1g} + B_{1g} + B_{2g} + [A_{2g}]$	$123(Z_{5+,5-}, M_{5+,5-}, A_{5+,5-}), 124(M_{5+,5-}), 125(Z_{5+,5-}), 127(Z_{5+,5-}),$ $129(Z_{5+,5-}), 131(M_{5+,5-}), 132(M_{5+,5-}), 134(A_{5+,5-}), 139(M_{5+,5-}),$ $140(M_{5+,5-}), 221(M_{5+,5-}, X_{5+,5-}^*), 223(M_{5+,5-}), 225(X_{5+,5-}^*), 226(X_{5+,5-}^*)$
$D_{4h} : A_{1g} + A_{2g} + B_{2g} + [B_{1g}]$	$127(M_{5+,5-}, A_{5+,5-}), 128(M_{5+,5-}), 135(M_{5+,5-}), 136(M_{5+,5-}), 138(A_{5+,5-})$
$C_{2h} : A_g + 2B_g + [A_g]$	$14(D_{1+2+,1-2-}^*, E_{1+2+,1-2-}^*), 64(R_{1+2+,1-2-})$
$D_{2h} : A_g + 2B_{ig} + [A_g]$	$55(S_{1+2+,1-2-,3+4+,3-4-}, R_{1+2+,1-2-,3+4+,3-4-}), 56(R_{1+2+,1-2-,3+4+,3-4-}),$ $58(S_{1+2+,1-2-,3+4+,3-4-}), 62(U_{1+4+,1-4-,2+3+,2-3-})$
$C_{4h} : A_g + 2B_g + [A_g]$	$83(Z_{3+4+,3-4-}, M_{3+4+,3-4-}, A_{3+4+,3-4-}),$ $84(M_{3+4+,3-4-}), 85(Z_{3+4+,3-4-}), 86(A_{3+4+,3-4-}), 87(M_{3+4+,3-4-})$
$D_{4h} : A_{1g} + 2B_{2g} + [A_{1g}]$	$127(M_{1+4+,1-4-,2+3+,2-3-}, A_{1+4+,1-4-,2+3+,2-3-}), 128(M_{1+4+,1-4-,2+3+,2-3-}),$ $135(M_{1+4+,1-4-,2+3+,2-3-}), 136(M_{1+4+,1-4-,2+3+,2-3-}), 138(A_{1+4+,1-4-,2+3+,2-3-})$
$S_6 : A_g + E_g + [A_g]$	$147(A_{2+3+,2-3-}), 148(T_{2+3+,2-3-}), 202(L_{2+3+,2-3-}^*), 203(L_{2+3+,2-3-}^*)$
$D_{3d} : A_{1g} + E_g + [A_{2g}]$	$162(A_{3+,3-}), 164(A_{3+,3-}), 166(T_{3+,3-}), 225(L_{3+,3-}^*), 227(L_{3+,3-}^*)$
$C_{6h} : A_g + E_{2g} + [A_g]$	$175(A_{3+5+,3-5-,4+6+,4-6-})$
$D_{6h} : A_{1g} + E_{2g} + [A_{2g}]$	$191(A_{5+,5-,6+,6-})$
$T_h : A_g + E_g + [A_g]$	$200(R_{2+3+,2-3-}), 201(R_{2+3+,2-3-}), 204(H_{2+3+,2-3-}), 206(H_{2+3+,2-3-})$
$O_h : A_{1g} + E_g + [A_{2g}]$	$221(R_{3+,3-}), 224(R_{3+,3-}), 229(H_{3+,3-})$

#### List of tables

Table.I contains real-space symmetry breaking  $\Gamma_{\mathbf{Q}} \otimes_A \Gamma_{\mathbf{Q}}$  for  $\mathbf{S}_1 \times \mathbf{S}_2$ , and  $\Gamma_{\mathbf{Q}} \otimes_S \Gamma_{\mathbf{Q}}$  for  $\mathbf{S}_1 \cdot \mathbf{S}_2$  &  $\mathbf{S}_1 \cdot \mathbf{S}_1 - \mathbf{S}_2 \cdot \mathbf{S}_2$  for 2D irreducible representations.

Table.II contains real-space crystal symmetry breaking of the coplanar state  $\mathbf{S}_1 \times \mathbf{S}_2$  of 2D irreducible representation  $\Gamma_{\mathbf{Q}}$ , obtained from  $\Gamma_{\mathbf{Q}} \otimes_A \Gamma_{\mathbf{Q}}$ . The resulting spin conductivities and material realizations in Magndata database are included.

Table.III contains tight-binding coefficients  $t_{x,z}$  for different primitive space groups with two inversion-invariant sublattices.

TABLE II. Real-space crystal symmetry breaking of the coplanar state  $\mathbf{S}_1 \times \mathbf{S}_2 // \hat{l}$  of 2D irreducible representation  $\Gamma_{\mathbf{Q}}$ , and the resulting spin conductivities. Point groups that preserve the wavevector  $\mathbf{Q}$  is included. Labels \* denote symmetries not along the conventional axis. For instance, 202L hosts 3-fold rotation along (111) rather than (001) direction. Metallic materials are marked in red. In hexagonal systems  $D_{3d}, D_{6h}, C_{6h}, S_6$ , the angle between x,y axes is  $120^\circ$ .

	$\Gamma_{\mathbf{Q}} \otimes_A \Gamma_{\mathbf{Q}}$	Space group & Wavevector	spin conductivity	materials
$D_{2h}$	$B_{1g}$	$53(R_{1+,1-}, U_{1+,1-})$	$\sigma_{xy}^l, \sigma_{yx}^l$	
$D_{2h}$	$B_{2g}$	$52(T_{1+,1-}), 58(T_{1+,1-}), 128(R_{1+,1-}), 136(R_{1+,1-})$	$\sigma_{xz}^l, \sigma_{zx}^l$	$\text{Cr}_2\text{ReO}_6$
$D_{2h}$	$B_{3g}$	$58(U_{1+,1-}), 60(S_{1+,1-})$	$\sigma_{yz}^l, \sigma_{zy}^l$	
$D_{3d}$	$A_{2g}$	$162(A_{3+,3-}), 164(A_{3+,3-}), 166(T_{3+,3-}), 225(L_{3+,3-}^*), 227(L_{3+,3-}^*)$	$\sigma_{xy}^l = -\sigma_{yx}^l$	$\text{AgFe}_3(\text{SO}_4)_2(\text{OD})_6$ $\text{KFe}_3(\text{OH})_6(\text{SO}_4)_2$ $\text{NaFe}_3(\text{SO}_4)_2(\text{OH})_6$ <b><math>\text{Gd}_2\text{Ti}_2\text{O}_7</math></b>
$D_{4h}$	$A_{2g}$	$123(A_{5+,5-}, M_{5+,5-}, Z_{5+,5-}), 124(M_{5+,5-}), 125(Z_{5+,5-}), 127(Z_{5+,5-}), 129(Z_{5+,5-}), 131(M_{5+,5-}), 132(M_{5+,5-}), 134(A_{5+,5-}), 139(M_{5+,5-}), 140(M_{5+,5-}), 221(M_{5+,5-}, X_{5+,5-}^*), 223(M_{5+,5-}), 225(X_{5+,5-}^*), 226(X_{5+,5-}^*)$	$\sigma_{xy}^l = -\sigma_{yx}^l$	<b><math>\text{U}_2\text{Rh}_2\text{Sn}, \text{U}_2\text{Ni}_2\text{In}</math></b> <b><math>\text{Yb}_2\text{Pd}_2\text{In}_{0.4}\text{Sn}_{0.6}</math></b>
$D_{4h}$	$B_{1g}$	$127(A_{5+,5-}, M_{5+,5-}), 128(M_{5+,5-}), 135(M_{5+,5-}), 136(M_{5+,5-}), 138(A_{5+,5-})$	$\sigma_{xx}^l = -\sigma_{yy}^l$	
$D_{6h}$	$A_{2g}$	$191(A_{5+,5-}, 6+, 6-)$	$\sigma_{xy}^l = -\sigma_{yx}^l$	
$O_h$	$A_{2g}$	$221(R_{3+,3-}), 224(R_{3+,3-}), 229(H_{3+,3-})$	0	
$C_{2h}$	$A_g$	$14(D_{1+2+,1-2-}^*, E_{1+2+,1-2-}^*), 64(R_{1+2+,1-2-})$	$\sigma_{xy}^l, \sigma_{yx}^l, \sigma_{xx}^l, \sigma_{yy}^l, \sigma_{zz}^l$	
$C_{4h}$	$A_g$	$83(A_{3+4+,3-4-}, M_{3+4+,3-4-}, Z_{3+4+,3-4-}), 84(M_{3+4+,3-4-}), 85(Z_{3+4+,3-4-}), 86(A_{3+4+,3-4-}), 87(M_{3+4+,3-4-})$	$\sigma_{xy}^l = -\sigma_{yx}^l, \sigma_{xx}^l = \sigma_{yy}^l; \sigma_{zz}^l$	
$C_{6h}$	$A_g$	$175(A_{3+5+,3-5-,4+6+,4-6-})$	$\sigma_{xy}^l = -\sigma_{yx}^l, \sigma_{xx}^l = \sigma_{yy}^l; \sigma_{zz}^l$	
$D_{2h}$	$A_g$	$55(R_{1+2+,1-2-,3+4+,3-4-}, S_{1+2+,1-2-,3+4+,3-4-}), 56(R_{1+2+,1-2-,3+4+,3-4-}), 58(S_{1+2+,1-2-,3+4+,3-4-}), 62(U_{1+4+,1-4-,2+3+,2-3-})$	$\sigma_{xx}^l, \sigma_{yy}^l, \sigma_{zz}^l$	$\text{Bi}_2\text{Fe}_4\text{O}_9, \text{AgMnVO}_4$ $\text{NaFePO}_4, \text{Ni}_2\text{SiO}_4$
$D_{4h}$	$A_{1g}$	$127(A_{1+4+,1-4-,2+3+,2-3-}, M_{1+4+,1-4-,2+3+,2-3-}), 128(M_{1+4+,1-4-,2+3+,2-3-}), 135(M_{1+4+,1-4-,2+3+,2-3-}), 136(M_{1+4+,1-4-,2+3+,2-3-}), 138(A_{1+4+,1-4-,2+3+,2-3-})$	$\sigma_{xx}^l = \sigma_{yy}^l; \sigma_{zz}^l$	$\text{BaNd}_2\text{PtO}_5, \text{Bi}_4\text{Fe}_5\text{O}_{13}\text{F}$
$S_6$	$A_g$	$147(A_{2+3+,2-3-}), 148(T_{2+3+,2-3-}), 202(L_{2+3+,2-3-}^*), 203(L_{2+3+,2-3-}^*)$	$\sigma_{xy}^l = -\sigma_{yx}^l, \sigma_{xx}^l = \sigma_{yy}^l; \sigma_{zz}^l$	$\text{Cu}_6(\text{SiO}_3)_6(\text{H}_2\text{O})_6$
$T_h$	$A_g$	$200(R_{2+3+,2-3-}), 201(R_{2+3+,2-3-}), 204(H_{2+3+,2-3-}), 206(H_{2+3+,2-3-})$	$\sigma_{xx}^l = \sigma_{yy}^l = \sigma_{zz}^l$	<b><math>\text{CaCu}_3\text{Ti}_4\text{O}_{12}</math></b>

TABLE III. Tight-binding coefficients for primitive space groups with two atoms per unit cell at the inversion center. Abbreviation  $c_i \equiv \cos k_i$ ,  $s_i \equiv \sin k_i$ ,  $c_{i/2} \equiv \cos \frac{k_i}{2}$ , and  $s_{i/2} \equiv \sin \frac{k_i}{2}$  applies. Prefactors are omitted from this table. For instance,  $s_y(s_x, s_z)$  in SG14 means  $t_{z1}s_y s_x + t_{z2}s_y s_z$ .

SG	$t_x(\mathbf{k})$	$t_z(\mathbf{k})$	SG	$t_x(\mathbf{k})$	$t_z(\mathbf{k})$
14(2a-2d)	$c_y/2(s_x s_z/2, c_z/2)$	$s_y(s_x, s_z)$	124(2b,2d)	$c_z/2$	$s_x s_y(c_x - c_y)$
53(2a-2d)	$c_x/2 c_z/2$	$s_y s_z$	127(2a,2b)	$c_x/2 c_y/2$	$s_x s_y(c_x - c_y)$
55(2a-2d)	$c_x/2 c_y/2$	$s_x s_y$	127(2c,2d)	$c_x/2 c_y/2$	$s_x s_y$
58(2a-2d)	$c_x/2 c_y/2 c_z/2$	$s_x s_y$	128(2a,2b)	$c_x/2 c_y/2 c_z/2$	$s_x s_y(c_x - c_y)$
83(2e,2f)	$c_x/2 c_y/2, s_x/2 s_y/2(c_x - c_y)$	$(c_x - c_y), s_x s_y$	131(2a,2b)	$c_z/2$	$(c_x - c_y)$
84(2a,2b)	$c_z/2$	$(c_x - c_y), s_x s_y$	131(2c,2d)	$c_x/2 c_y/2 c_z/2$	$(c_x - c_y)$
84(2c,2d)	$c_x/2 c_y/2 c_z/2, s_x/2 s_y/2 c_z/2$	$(c_x - c_y), s_x s_y$	132(2a,2c)	$c_z/2$	$s_x s_y$
123(2e,2f)	$c_x/2 c_y/2$	$(c_x - c_y)$	136(2a,2b)	$c_x/2 c_y/2 c_z/2$	$s_x s_y$
			223(2a)	$c_x/2 c_y/2 c_z/2$	$(c_x - c_y)(c_y - c_z)(c_z - c_x)$